Time-Resolved Energy-Momentum Spectroscopy of Electric and Magnetic Dipole Transitions in Cr^{3+}:MgO

Sinan Karaveli,[†] Shutong Wang,[‡] Gang Xiao,[‡] and Rashid Zia[†,‡,*]

[†]School of Engineering and [‡]Department of Physics, Brown University, Providence, Rhode Island 02912, United States

ABSTRACT Due to the recent interest in magnetic light-matter interactions, the magnetic dipole (MD) transitions in lanthanide ions have been studied for potential applications in nano-optics. Similar to lanthanide ions, transition-metal ions also exhibit strong MD emission at room temperature, but their prominent MD zero-phonon lines are often accompanied by significant electric dipole (ED) sideband emission. Here, we extend energy-momentum spectroscopy to time-resolved measurements, and use this technique to quantify the ED and MD contributions to light emission from trivalent chromium doped magnesium oxide (Cr^{3+}:MgO). This allows us to differentiate the MD $^2E \rightarrow {}^4A_2$ zero-phonon line from phonon-assisted $^2E \rightarrow {}^4A_2$ and $^4T_2 \rightarrow {}^4A_2$ ED sidebands. We also demonstrate how the relative intensities of the sharp MD zero-phonon line and the broad ED sidebands can be used as a qualitative measure of the MD and ED local density of optical states.

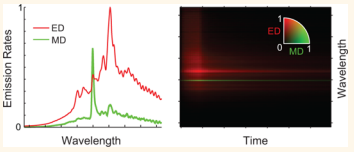

KEYWORDS: light-matter interactions · magnetic dipole transitions · time-resolved spectroscopy · transition-metal ions · local density of optical states (LDOS) · photoluminescence

Building on advances in the field of metamaterials, researchers have recently demonstrated how the magnetic response from man-made nanostructures can be used to map optical-frequency magnetic fields[1−3] and study magnetic light-matter interactions.[4−6] Together with these developments, there has been renewed interest in the MD transitions of lanthanide ions for use in nano-optics as natural probes of the magnetic component of light.[7−9] Experimental studies have shown how the MD emission from Eu^{3+} ions can be enhanced,[10−12] and numerical simulations have identified metal and dielectric nanostructures that could enhance MD emission from the 1.55 μm telecom line in Er^{3+} ions.[13−16] Recent calculations have also identified nearly 2000 optical-frequency MD emission lines in the trivalent lanthanide series.[17]

To experimentally characterize the magnetic nature of light emission in lanthanide ions, Taminiau *et al.*[9] recently used energy- and momentum-resolved spectroscopy to distinguish ED and MD transitions and to quantify their intrinsic spontaneous emission rates. This energy-momentum spectroscopy technique revealed a set of spectrally close ED and MD emission lines in Eu^{3+} near 580 nm that were subsequently used as nanoscale probes of the ED and MD local density of optical states (LDOS). To extend this method to other wavelengths, it would be advantageous to identify additional systems in which MD transitions appear in close spectral proximity to ED transitions.

Transition-metal doped crystals represent another class of solid-state emitters that exhibit strong MD transitions and could fulfill this purpose. Similar to the intra-4f transitions of lanthanide ions, the intra-3d transitions of transition-metal ions within high-symmetry (*e.g.*, octahedral) sites are ED forbidden but MD allowed.[18,19] Unlike the 4f orbitals of lanthanide ions though, the 3d orbitals of transition-metal ions are not shielded by closed outer orbitals. Consequently, transition-metal ions interact more strongly with their crystal host, which causes the emission from purely electronic transitions (also called zero-phonon lines) to be accompanied by vibronic (phonon-assisted) sidebands, and provide a complex system with rich luminescent properties.

In this paper, we quantify the MD contribution to room temperature emission from trivalent chromium (Cr^{3+}) doped magnesium oxide (MgO) thin films. Using continuous and time-resolved energy-momentum spectroscopy, we characterize light emission from the Cr^{3+}:MgO $^2E \rightarrow {}^4A_2$ zero-phonon line (ZPL) as well as the related $^2E \rightarrow {}^4A_2$ and

* Address correspondence to rashid_zia@brown.edu.

Received for review May 21, 2013 and accepted July 23, 2013.

Published online July 23, 2013
10.1021/nn402568d

$^4T_2 \rightarrow {}^4A_2$ sidebands near 700 nm. We confirm previous findings that the $^2E \rightarrow {}^4A_2$ ZPL is mediated by MD transitions, whereas the sidebands are mediated by ED transitions. In contrast to other methods,[20−22] energy-momentum spectroscopy does not require single crystal samples with known crystallographic orientation and can be used to study polycrystalline thin films. It is also well-suited for time-resolved studies. Using a time-gated intensified camera to acquire energy-momentum spectra, we characterize the time evolution of ED and MD emission and use the MD ZPL emission as an internal reference to separate the fast- and slow-decaying ED transitions. Furthermore, we show that the observed ZPL-to-sideband ratio can be used as a qualitative measure of the relative MD/ED LDOS, and demonstrate that simple optical engineering can be used to selectively enhance ZPL emission.

RESULTS AND DISCUSSION

At low concentrations Cr^{3+} is a substitutional dopant that replaces Mg^{2+} within the octahedral sites of the cubic MgO crystal. In these sites, the ground state for the $3d^3$ configuration of Cr^{3+} is $^4A_2$, whereas the first excited state is ^2E and the second excited state is $^4T_2$ (see inset in Figure 1).[18] Figure 1 shows the room temperature emission spectrum of a 22 nm Cr^{3+}-doped MgO thin film deposited on a quartz substrate. The sharp feature near 699 nm corresponds to the $^2E \rightarrow {}^4A_2$ ZPL, whereas the emission peaks at longer and shorter wavelengths correspond to the Stokes and anti-Stokes phonon sidebands, respectively. (Although the $^2E \rightarrow {}^4A_2$ ZPL is generally described in the literature by its low temperature wavelength of 698.1 nm, this line red-shifts with increasing temperature and is close to 699 nm at room temperature.[23])

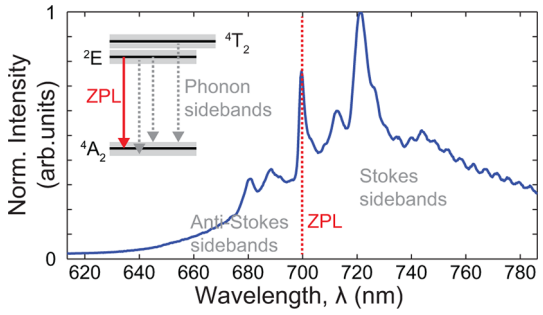

Figure 1. Room temperature emission spectrum of Cr^{3+}:MgO thin film under 488 nm laser excitation. Inset: Energy level schematic of Cr^{3+} ions in octahedral sites.

The MD nature of the $^2E \rightarrow {}^4A_2$ ZPL has been previously determined by measuring its Zeeman splitting in a weakly doped Cr^{3+}:MgO crystal at liquid nitrogen temperature and comparing it to the theoretically calculated Zeeman patterns for ED and MD transitions.[20] On the other hand, optically detected magnetic resonance (ODMR) measurements have shown, again at liquid nitrogen temperature, that the phonon sideband emission is consistent with ED transitions mediated by the odd parity, T_{1u}, phonon vibrations.[21] These and other methods[22] used to determine the nature of the observed transitions rely on cryogenic temperatures to minimize broadening effects such that the ZPL and sidebands are spectrally well separated. Furthermore, at higher temperatures, it is known that emission from the $^4T_2 \rightarrow {}^4A_2$ transition, which partially overlaps with the $^2E \rightarrow {}^4A_2$ transition, becomes increasingly important.[24,25] To enable the use of Cr^{3+}:MgO as a room temperature probe of the ED and MD LDOS, we must first quantify the different ED and MD contributions to the emission spectrum seen in Figure 1.

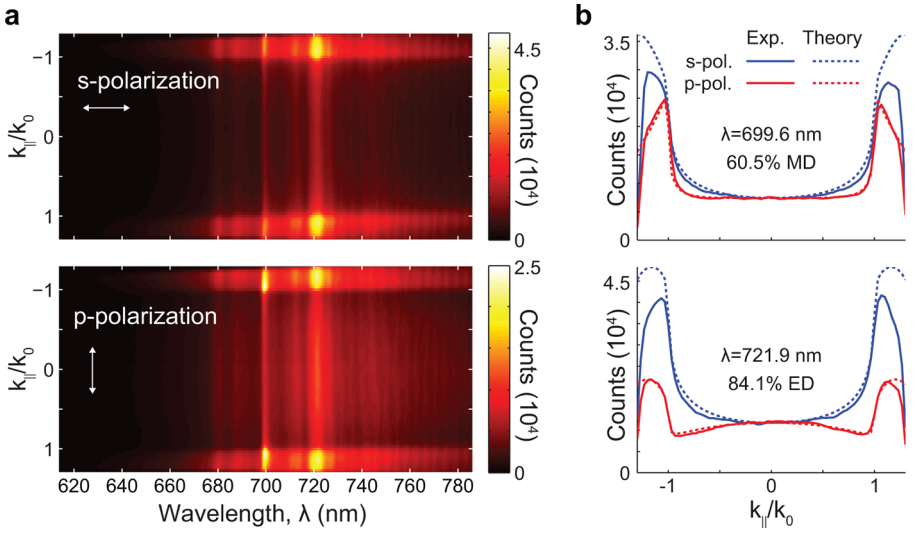

Figure 2. Characterization by energy-momentum spectroscopy under continuous illumination. (a) Experimental energy- and momentum-resolved spectra for s- and p-polarization, respectively. (b) Momentum cross sections of the experimental data (solid lines) and theoretical fits (dashed lines) taken at 699.6 and 721.9 nm corresponding to the ZPL and the phonon sideband peak, respectively.

For this purpose, we first employed the energy-momentum spectroscopy technique described in ref 9 using continuous illumination. Figure 2a shows the steady-state energy- and momentum-resolved spectra for the s- and p-polarized emission of Cr^{3+}:MgO. To analyze this system, we assume that emission originates from isotropic ED and MD emitters located at the center of a 22 nm MgO thin film with a refractive index of 1.73. As described in the Methods, we fit the p-polarized momentum cross sections at each wavelength to theoretical calculations and obtain the relative ED and MD contributions. For comparison, two experimental cross sections with high MD and high ED contributions are shown in Figure 2b together with the fit results. In addition to the fractional ED and MD contributions, this analysis also provides the spectrally resolved intrinsic ED and MD emission rates shown in Figure 3.

Note that the most pronounced MD contribution to emission near 699 nm corresponds to the $^2E \rightarrow {}^4A_2$ ZPL, whereas the sidebands are clearly dominated by ED emission. These results also show that, at room temperature, the MD ZPL is not spectrally distinct but is in fact superimposed on the broad ED sideband; the MD contributions at 699.6 nm corresponds to ~60% of the intrinsic emission rate, and the remaining ~40% is ED emission. As discussed above, it is known from the literature that the $^2E \rightarrow {}^4A_2$ emission band partially overlaps with the $^4T_2 \rightarrow {}^4A_2$ emission band of Cr^{3+}, which might account for the large ED signature we observe in Figure 3. To characterize the extent to which the $^4T_2 \rightarrow {}^4A_2$ transition contributes to observed ED emission, we performed time-resolved photoluminescence studies of Cr^{3+}:MgO emission. These include standard time-resolved measurements of the energy spectra as well as time-gated measurements of the full energy-momentum spectra.

Using pulsed excitation and a gated intensified camera, we first measured the photoluminescence energy spectrum as a function of time. The resulting time-dependent emission spectra are shown in Figure 4a (see Supporting Information for a movie of the time-varying energy spectra). To highlight the temporal and spectral changes, Figure 4b,c provides normalized cross sections for different times and wavelengths. During the excitation pulse, we observe a rapid increase in emission at long wavelengths (>750 nm), which then decreases significantly once the pump pulse ends at $t = 0.6$ ms. This initial fast rise and fall suggests that part of the broad emission results from a different excited state that exhibits a short (<100 μs) lifetime. On the other hand, the ZPL emission from the $^2E \rightarrow {}^4A_2$ transition continues to radiate long after the end of the excitation pulse and decays with a much longer lifetime (>1 ms).

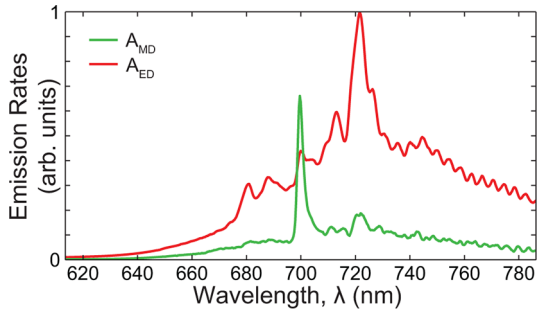

Figure 3. Spectrally resolved ED and MD emission rates, A_{ED} (red) and A_{MD} (green), deduced from theoretical fits to the experimental energy-momentum spectra shown in Figure 2.

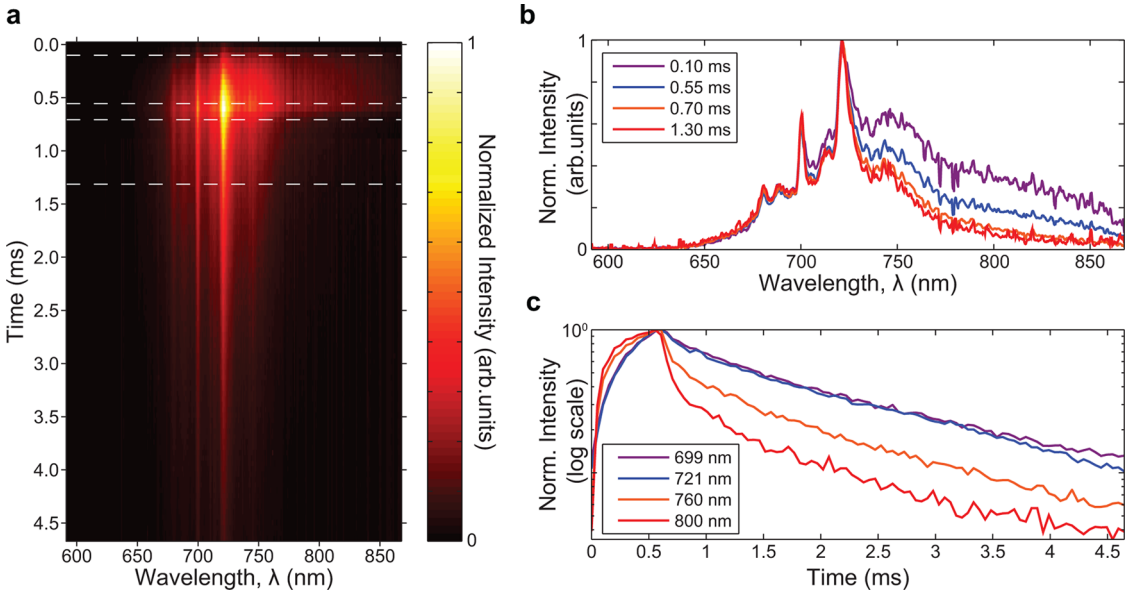

Figure 4. Time-resolved energy spectra of Cr^{3+}:MgO. (a) Color plot of Cr^{3+}:MgO emission as a function of time and wavelength. (b) Normalized emission spectra cross sections taken at different times indicated by white dashed lines in (a). (c) Normalized intensity as a function of time at different wavelengths.

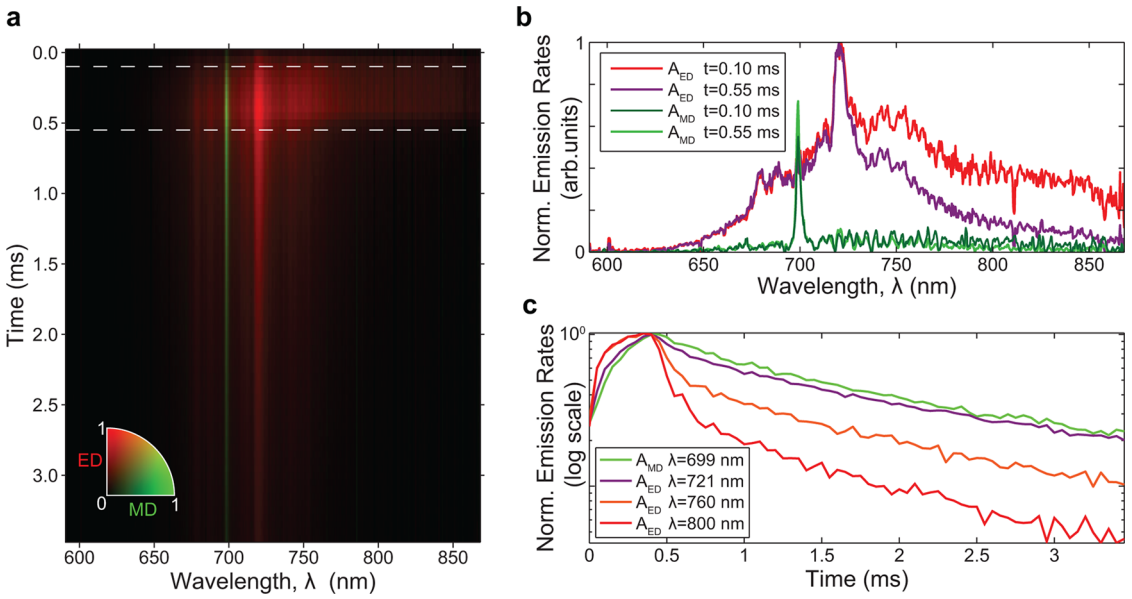

Figure 5. Spectrally and temporally resolved ED and MD emission rates of Cr^{3+}:MgO. (a) False color plot of Cr^{3+}:MgO emission rates, A_{ED} (red) and A_{MD} (green), as a function of time and wavelength. (b) Spectrally resolved emission rate cross sections normalized to the A_{ED} peak near 721 nm for the $t = 0.1$ ms and $t = 0.55$ ms timestamps indicated by white dashed lines in (a). (c) Time decay traces for the emission rates normalized to the maximum count position ($t = 0.4$ ms) at select wavelengths for A_{MD} (699 nm) and A_{ED} (721 nm, 760 nm, and 800 nm) emission.

Next, we introduced a Bertrand lens and polarizer into the optical path to acquire the s- and p-polarized energy-momentum spectra as a function of time for 50 μs intervals (see Methods for details on the experimental setup and Supporting Information for a movie of the time-varying energy-momentum spectra). As described in the Methods, we then fit the momentum distribution of the acquired p-polarized data with theory at each wavelength and time step, which allowed us to characterize the dynamic evolution of the ED and MD emission rates. The fit results are summarized in Figure 5a where the false-color plot shows the relative ED and MD emission rates as a function of both time and wavelength (see Supporting Information for a movie of the time-varying rates). These spectrally and temporally resolved emission rates are the product of the time-varying excited state population with the spectrally resolved emission rates for ED and MD transitions. Select wavelength and time cross sections are highlighted in Figure 5, panels b and c for direct comparison. We again see that the only significant MD contribution comes from the ZPL near 699 nm which decays slowly. ED emission, on the other hand, exhibits both a fast- and slow-decaying contribution as can be seen from Figure 5b. From this time-resolved characterization, we can also calculate the MD percentage at 699 nm as a function of time; whereas MD emission accounts for ~56% of the total emission rate at the very start of the excitation pulse, this value increases over the duration of the pulse to ~66% and continues to rise until it reaches a value of ~74% at 2 ms after the pulse ends. This indicates that, although some of the ED emission at 699 nm is due to fast-decaying EDs, the ZPL still has significant overlap with a slow-decaying ED emission process.

Having characterized the ED and MD intrinsic rates as a function of time and wavelength, we can also separate the fast and slow ED emission processes. Note that the MD ZPL and the slow ED component decay at the same rate, as evidenced by the green (MD) and purple (ED) time traces in Figure 5c. Consequently, the intrinsic MD ZPL emission can be used as an internal reference for the slow-decaying processes. We obtain the slow-decaying intrinsic ED emission spectra by integrating Figure 5a for $t > 1$ ms and normalizing it to the integrated MD ZPL emission for the same time range. We then scale this spectrum with the MD ZPL emission at each time bin to model the time evolution of the slow-decaying ED process. Subtracting this slow-decaying ED component from the total ED emission rates shown in Figure 5a allows us to isolate the fast-decaying ED emission process. As an example, Figure 6 shows the spectrally resolved ED emission rates separated into fast- and slow-decaying components, together with the reference MD emission.

The fast-decaying emission component has been previously attributed to the $^4T_2 \rightarrow {}^4A_2$ emission originating from Cr^{3+} ions in sites with orthorhombic symmetry.[24,25] Although MgO is a cubic crystal with purely octahedral sites, the replacement of divalent Mg^{2+} by trivalent Cr^{3+} results in charge compensation vacancies, which can lower the site symmetry from octahedral to orthorhombic and tetragonal.[18] In orthorhombic sites, the crystal fields are effectively reduced such that the $^4T_2$ excited state has a lower energy than the ^2E excited state.[25] (This is equivalent to

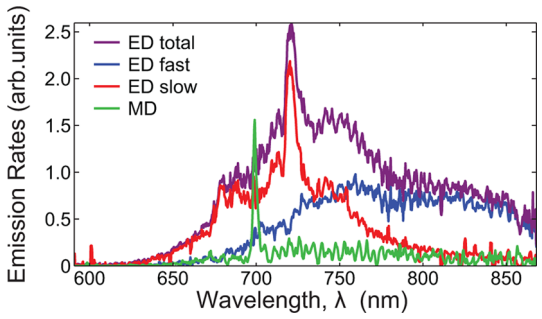

Figure 6. Example decomposition of the total ED emission rates (Figure 5a at t = 200 μs) into slow- and fast-decaying components together with the MD emission rate used as a reference for the slow-decaying ED process.

a movement toward the left on the standard Tanabe-Sugano diagram for the $3d^3$ configuration.[19]) Consequently, emission from ions in these sites is dominated by the broad spin-allowed $^4T_2 \rightarrow {}^4A_2$ transition centered at ~800 nm. The time-resolved characterization reveals that this fast-decaying component is purely of ED character, as one would expect from its speed and site symmetry. In tetragonal sites, the ^2E state is still the first excited state, but its ZPL emission is significantly decreased at room temperature and disappears above 300 K.[25] Our results are in agreement with these assertions as we do not observe any emission peaks near 703 nm that could be associated with the $^2E \rightarrow {}^4A_2$ ZPL of tetragonal site ions.

The slow-decaying broad emission overlapping with the $^2E \rightarrow {}^4A_2$ ZPL and its ED sideband, on the other hand, has been attributed to the $^4T_2 \rightarrow {}^4A_2$ emission from octahedral and tetragonal site Cr^{3+} ions.[24,25] At room temperature, the small energy separation between ^2E and $^4T_2$ states results in significant $^2E \rightarrow {}^4T_2$ energy transfer followed by $^4T_2 \rightarrow {}^4A_2$ emission that spectrally overlaps with the $^2E \rightarrow {}^4A_2$ transition. Consequently, we believe the majority of the slow-decaying ED emission that we observe in Figures 5 and 6 is due to the $^4T_2 \rightarrow {}^4A_2$ transitions from octahedral and tetragonal site Cr^{3+} ions.

Even though the MD ZPL emission of Cr^{3+} overlaps with a broad ED emission band, the ZPL-to-sideband ratio can still be used as a qualitative probe of the relative MD to ED LDOS. As a simple example, Figure 7a shows the emission spectrum of the Cr^{3+}:MgO thin film shown in Figure 1 together with the emission spectrum of an identical sample that has been coated with an additional 90 nm MgO thin film. Both spectra have been normalized to the intensity of the ED sideband peak located at 721 nm. Whereas most of the emission spectrum remains unchanged for the coated sample, the MD ZPL is significantly enhanced compared to the ED sideband. This large difference is due to the fact that the ED LDOS is higher than the MD LDOS within a high-refractive-index thin film.[9] Consequently, for the bare 22 nm Cr^{3+}:MgO thin film, the ED sideband is

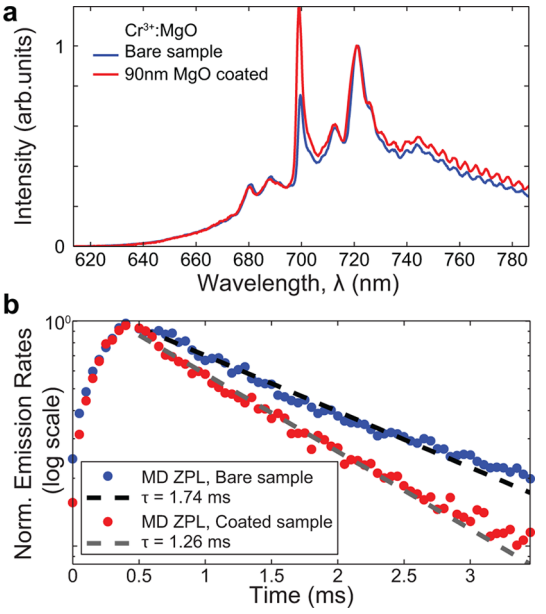

Figure 7. ZPL to sideband ratio as a qualitative measure of the MD/ED LDOS. (a) Comparison of a bare 22 nm Cr^{3+}:MgO thin film emission spectrum to an identical sample coated with an additional 90 nm MgO overcoat. The contrast of the ZPL over the sideband emission is enhanced as the ratio of the MD to ED LDOS increases with the addition of the overcoat layer. (b) Time-resolved MD ZPL emission rates for the bare and coated samples normalized to maximum values. Fitting to single exponential decays (dashed lines) shows that the lifetime decreases from 1.76 ± 0.06 ms for the bare sample to 1.26 ± 0.05 ms for the coated sample.

enhanced compared to the MD ZPL. Coating the Cr^{3+}:MgO layer with an additional 90 nm of MgO, however, reverses this situation and enhances the MD ZPL more so than the ED sideband. This increased contrast of the ZPL in such engineered optical environments could also be useful for fundamental studies of other ZPLs that overlap with much stronger sidebands and are thus difficult to detect.

To confirm that the increased ZPL-to-sideband ratio shown in Figure 7a is due to LDOS modification, we also measured the lifetime of the ^2E excited state. To this end, we performed time-resolved energy-momentum spectroscopy measurements on both the bare and coated samples. As shown in Figure 7b, this allows us to isolate the dynamics of the $^2E \rightarrow {}^4A_2$ MD ZPL transition and thus monitor the time decay of the ^2E excited state. Consistent with an increased total LDOS, we observe that the lifetime decreases from ~1.74 ms for the bare sample to ~1.26 ms for the coated sample. However, this excited state lifetime is a complicated function that depends on all decay mechanisms from the ^2E state, including both MD and ED direct emission (*i.e.*, the $^2E \rightarrow {}^4A_2$ MD ZPL and the $^2E \rightarrow {}^4A_2$ ED phonon sidebands) as well as energy transfer to the $^4T_2$ state, which is followed by $^4T_2 \rightarrow {}^4A_2$ ED emission. As ED transitions dominate the emission process (see Figure 5a), lifetime variations should mainly follow that of the associated ED LDOS. For comparison, we calculated the

LDOS modifications for isotropic ED and MD transitions emitting at 700 nm.[26] Assuming unity quantum efficiency, the calculated ratios of the lifetimes should be $\tau_{ED}^{coated}/\tau_{ED}^{bare} = 0.81$ and $\tau_{MD}^{coated}/\tau_{MD}^{bare} = 0.51$ for pure ED and MD transitions, respectively. As expected, the measured lifetime ratio ($\tau^{coated}/\tau^{bare} = 1.26/1.74 = 0.72$) lies between these values and is close to that of the dominant ED transitions. Consistent with the enhanced MD ZPL emission shown in Figure 7a, these calculations also show that the MD LDOS nearly doubles with the addition of the overcoat, whereas the ED LDOS increases by only 23%. This highlights the probative value of the ZPL-to-sideband intensity ratio, especially when collected over a broad range of modes (*e.g.*, in this case over NA = 1.3). Although the lifetime can be difficult to interpret by itself, the emission intensity ratio of the MD ZPL relative to the ED sideband can provide a qualitative gauge of the MD to ED LDOS.

CONCLUSION

In conclusion, we have experimentally characterized the different ED and MD contributions to the room temperature emission spectrum of Cr^{3+}:MgO thin films. Specifically, we expanded the energy-momentum spectroscopy method to the time domain, which allowed us to quantify the dynamic evolution of the MD $^2E \rightarrow {}^4A_2$ ZPL and its associated ED sidebands as well as the ED emission originating from $^4T_2 \rightarrow {}^4A_2$ transitions from Cr^{3+} ions in different ion sites.

MD emission in transition-metal ions is not limited to the $^2E \rightarrow {}^4A_2$ ZPL of Cr^{3+}. Many other transition-metal ions support strong MD emission lines over a wide range of wavelengths. For example, Mn^{4+} and V^{2+} ions in MgO, which share the $3d^3$ electronic configuration of Cr^{3+}, also exhibit MD emission from their ZPLs at 654 and 870 nm, respectively.[23,27] In addition to nanometer scale thin films, transition-metal doped MgO can also be synthesized in the form of highly regular cubic nanocrystals.[28,29] Furthermore, as these ions interact strongly with their electronic surrounding, their emission spectrum can differ sharply from one host crystal to another. For example, while the $^3T_2 \rightarrow {}^3A_2$ ZPL of Ni^{2+} occurs near 1.3 μm in MgO, the same transition is shifted to near 1.55 μm in MgF_2.[30] Consequently, the MD emission of transition-metal ions could serve as local probes of the optical-frequency magnetic field over a broad spectral range.

To this end, we have demonstrated how time-resolved energy-momentum spectroscopy can be used to characterize and quantify the different ED and MD contributions to room temperature transition-metal ion luminescence. We have also shown a simple demonstration of how the relative intensity of a sharp MD ZPL as compared to broad ED sidebands can be used to gauge the relative ratio of the MD and ED LDOS. Better engineered optical environments leveraging the difference between the ED and MD LDOS could significantly increase the ZPL-to-sideband contrast. Tailoring the LDOS to enhance MD ZPLs while simultaneously suppressing ED sidebands might prove useful for quantum information processing applications, where accessing the ZPL is particularly important to minimize decoherence. Building on the recent study of different ED orientations in the organic semiconductor PTCDA,[31] the distinct radiation patterns of ED and MD transition could also be used to isolate distinct populations and selectively access the ZPL for dynamic study using conventional single-photon avalanche photodiodes.

Finally, the time-resolved nature of this study can also be extended to other recent applications of energy-momentum spectroscopy for the characterization of directional Raman scattering[32] and luminescent excitons in layered nanomaterials.[31] Although the present work focused on the relatively slow dynamics of the long-lived Cr^{3+} states, intensified cameras such as the one used here can be gated down to sub-500 ps. Thus, time-resolved energy-momentum spectroscopy can be readily used to study faster dynamics, such as the reorientation of excitons in organic semiconductors.

METHODS

Sample Fabrication and Experimental Setup. The 22 nm chromium-doped magnesium oxide thin-films were deposited onto quartz coverslips *via* electron beam evaporation of Cr^{3+}:MgO (0.1 atom %) pellets. Cr^{3+} ions were excited with a 488 nm pump laser (Coherent Innova 300C) and their photoluminescence was collected through a 1.3 NA 100× microscope objective in an inverted microscope (Nikon TE2000). For standard spectral measurements, the collected emission was focused to the entrance slit of an imaging spectrograph (Princeton Instruments, SP2300i) and detected with either a CCD camera for continuous-wave measurements (Princeton Instruments, ProEM) or a gated intensified CCD camera (Princeton Instruments, PI-MAX4 1024i RB) for time-resolved measurements. For energy-momentum measurements, a 50 mm Bertrand lens was placed between the spectrograph and microscope to image the back-focal plane (BFP) of the objective onto the entrance slit as described in detail in ref 9. Time-resolved photoluminescence experiments were carried out with pulsed 488 nm excitation obtained using a mechanical chopper (Stanford Research, SR530). To measure the luminescence as a function of delay time following pulsed excitation, the PI-MAX4 intensified camera was gated at ~50 μs intervals and sampled for repeated excitation cycles. The peak count rates for the timed-resolved energy-momentum measurements presented here were on the order of 20 kHz per pixel, which corresponds to one count per gated acquisition per pixel.

Fitting Procedure. To quantify the ED and MD contributions, we use the formalism derived in ref 9 to fit the time-resolved energy-momentum intensity spectra to a superposition of ED and MD emission:

$$I^{s,p}(\omega, k_{||}, t) = C[\tilde{\rho}_{ED}^{s,p}(\omega, k_{||})A_{ED}(\omega, t) + \tilde{\rho}_{MD}^{s,p}(\omega, k_{||})A_{MD}(\omega, t)] \quad (1)$$

In this expression, C is a proportionality constant that depends on experimental parameters, *e.g.*, the excitation efficiency and

ion density. $\tilde{\rho}_{ED}^{s,p}(\omega, k_{||})$ and $\tilde{\rho}_{MD}^{s,p}(\omega, k_{||})$ are the normalized ED and MD LDOS for which explicit expressions are provided in Supplementary Equations S6−S14 of ref 9. $A_{ED}(\omega,t)$ and $A_{MD}(\omega,t)$ are the spectrally and temporally resolved ED and MD spontaneous emission rates in a bulk medium; they represent the product of the intrinsic emission rates (*i.e.*, the spectrally resolved Einstein A coefficients, $A_{ED}(\omega)$ and $A_{MD}(\omega)$) and the time-varying excited state populations for the active ion sites (*e.g.*, $n^{oct}(t)$, $n^{tet}(t)$, and $n^{rhomb}(t)$). Explicitly, for Cr^{3+}:MgO at room temperature, the MD rate mainly includes contributions from octahedral sites and, to a lesser extent, tetragonal sites, $A_{MD}(\omega,t) = A_{MD}^{oct}(\omega)n^{oct}(t) + A_{MD}^{tet}(\omega)n^{tet}(t)$, whereas the ED rate can include contributions from octahedral, tetragonal, and orthorhombic sites, $A_{ED}(\omega,t) = A_{ED}^{oct}(\omega)n^{oct}(t) + A_{ED}^{tet}(\omega)n^{tet}(t) + A_{ED}^{rhomb}(\omega)n^{rhomb}(t)$. Since the system under study is clearly inhomogeneous (*i.e.*, Cr^{3+} ions in different sites exhibit distinct spectra and dynamics), the spectrally and temporally resolved emission rates are a complex and evolving function that depends on both the emitters and optical environment. Nevertheless, the fit values for A_{ED} and A_{MD} obtained at each wavelength (and time step for time-resolved measurements) provide a direct measure of the ED and MD contributions to light emission.[9] Least squares fits to eq 1 were performed on the p-polarized data, whereas the s-polarized theoretical curves in Figure 2b were obtained from the p-polarized fits without any additional parameters and are shown for completeness.

Conflict of Interest: The authors declare no competing financial interest.

Acknowledgment. The authors thank S. Cueff, C. Dodson, M. Jiang, J. Kurvits, D. Li, and D. Pacifici for helpful discussions. Financial support for this work was provided by the Air Force Office of Scientific Research (MURI award FA-9550-12-1-0488) and by the National Science Foundation (CAREER award EECS-0846466 and DMR-0907353).

Supporting Information Available: Movies are provided of the time-resolved energy spectra (shown in Figure 4) as well as the p-polarized time-resolved energy-momentum spectra and inferred time-varying emission rates (shown in Figure 5) deduced from theoretical fits to experimental momentum cross section as a function of time and wavelength. This material is available free of charge *via* the Internet at http://pubs.acs.org.

REFERENCES AND NOTES

1. Burresi, M.; van Oosten, D.; Kampfrath, T.; Schoenmaker, H.; Heideman, R.; Leinse, A.; Kuipers, L. Probing the Magnetic Field of Light at Optical Frequencies. *Science* **2009**, *326*, 550–553.
2. Kihm, H. W.; Koo, S. M.; Kim, Q. H.; Bao, K.; Kihm, J. E.; Bak, W. S.; Eah, S. H.; Lienau, C.; Kim, H.; Nordlander, P.; *et al.* Bethe-Hole Polarization Analyser for the Magnetic Vector of Light. *Nat. Commun.* **2011**, *2*, 451.
3. Kihm, H. W.; Kim, J.; Koo, S.; Ahn, J.; Ahn, K.; Lee, K.; Park, N.; Kim, D.-S. Optical Magnetic Field Mapping using a Subwavelength Aperture. *Opt. Express* **2013**, *21*, 5625–5633.
4. Burresi, M.; Kampfrath, T.; van Oosten, D.; Prangsma, J. C.; Song, B. S.; Noda, S.; Kuipers, L. Magnetic Light-Matter Interactions in a Photonic Crystal Nanocavity. *Phys. Rev. Lett.* **2010**, *105*, 123901.
5. Vignolini, S.; Intonti, F.; Riboli, F.; Balet, L.; Li, L. H.; Francardi, M.; Gerardino, A.; Fiore, A.; Wiersma, D. S.; Gurioli, M. Magnetic Imaging in Photonic Crystal Cavities. *Phys. Rev. Lett.* **2010**, *105*, 125902.
6. Ameling, R.; Giessen, H. Cavity Plasmonics: Large Normal Mode Splitting of Electric and Magnetic Particle Plasmonics Induced by a Photonic Microcavity. *Nano Lett.* **2010**, *10*, 4394–4398.
7. Noginova, N.; Zhu, G.; Mavy, M.; Noginov, M. A. Magnetic Dipole Based Systems for Probing Optical Magnetism. *J. Appl. Phys.* **2008**, *103*, 07E901.
8. Noginova, N.; Barnakov, Y.; Li, H.; Noginov, M. A. Effect of Metallic Surface on Electric Dipole and Magnetic Dipole Emission Transitions in Eu^{3+} Doped Polymeric Film. *Opt. Express* **2009**, *17*, 10767–10772.
9. Taminiau, T. H.; Karaveli, S.; van Hulst, N. F.; Zia, R. Quantifying the Magnetic Nature of Light Emission by Energy Momentum Spectroscopy. *Nat. Commun.* **2012**, *3*, 979.
10. Karaveli, S.; Zia, R. Strong Enhancement of Magnetic Dipole Emission in a Multilevel Electronic System. *Opt. Lett.* **2010**, *35*, 3318–3320.
11. Karaveli, S.; Zia, R. Spectral Tuning by Selective Enhancement of Electric and Magnetic Dipole Emission. *Phys. Rev. Lett.* **2011**, *106*, 193004.
12. Ni, X.; Naik, G. V.; Kildishev, A. V.; Barnakov, Y.; Boltasseva, A.; Shalaev, V. M. Effect of Metallic and Hyperbolic Metamaterial Surfaces on Electric and Magnetic Dipole Emission Transitions. *Appl. Phys. B: Laser Opt.* **2011**, *103*, 553–558.
13. Feng, T.; Zhou, Y.; Liu, D.; Li, J. Controlling Magnetic Dipole Transition with Magnetic Plasmonic Structures. *Opt. Lett.* **2011**, *36*, 2369–2371.
14. Rolly, B.; Bebey, B.; Bidault, S.; Stout, B.; Bonod, N. Promoting Magnetic Dipolar Transition in Trivalent Lanthanide Ions with Lossless Mie Resonances. *Phys. Rev. B* **2012**, *85*, 245432.
15. Schmidt, M. K.; Esteban, R.; Sáenz, J. J.; Suárez-Lacalle, I.; Mackowski, S.; Aizpurua, J. Dielectric Antennas—A Suitable Platform for Controlling Magnetic Dipolar Emission. *Opt. Express* **2012**, *20*, 13636–13650.
16. Hein, S. M.; Giessen, H. Tailoring Magnetic Dipole Emission with Plasmonic Split-Ring Resonators. *Phys. Rev. Lett.* **2013**, *111*, 026803.
17. Dodson, C. M.; Zia, R. Magnetic Dipole and Electric Quadrupole Transitions in the Trivalent Lanthanide Series: Calculated Emission Rates and Oscillator Strengths. *Phys. Rev. B* **2012**, *86*, 125102.
18. Henderson, B.; Imbusch, G. F. *Optical Spectroscopy of Inorganic Solids*; Oxford University Press: Oxford, 2006.
19. Sugano, S.; Tanabe, Y.; Kamimura, H. *Multiplets of Transition-Metal Ions in Crystals*; Academic Press: New York, 1970.
20. Sugano, S.; Schawlow, A. L.; Varsanyi, F. Zeeman Effect of the Purely Cubic Field Fluorescence Line of MgO:Cr^{3+} Crystals. *Phys. Rev.* **1960**, *120*, 2045–2053.
21. McDonaght, C. M.; Henderson, B.; Imbusch, G. F. Optical Detection of Magnetic Resonance in the Vibronic Sidebands of R and N Lines in MgO:Cr^{3+}. *J. Phys. C: Solid State Phys.* **1980**, *13*, 6025–6031.
22. Imbusch, G. F.; Schawlow, A. L.; May, A. D.; Sugano, S. Fluorescence of MgO:Cr^{3+} Ions in Noncubic Sites. *Phys. Rev.* **1965**, *140*, A830–A838.
23. Imbusch, G. F.; Yen, W. M.; Schawlow, A. L.; McCumber, D. E.; Sturge, M. D. Temperature Dependence of the Width and Position of the $^2E \rightarrow {}^4A_2$ Fluorescence Lines of Cr^{3+} and V^{2+} in MgO. *Phys. Rev.* **1964**, *133*, A1029–A1034.
24. Castelli, F.; Forster, L. S. Fluorescence ($^4T_2 \rightarrow {}^4A_2$) and Phosphorescence ($^2E \rightarrow {}^4A_2$) in MgO:$Cr^{3+}$. *Phys. Rev. B* **1975**, *11*, 920–928.
25. Henry, M. O.; Larkin, J. P.; Imbusch, G. F. Nature of the Broadband Luminescence Center in MgO:Cr^{3+}. *Phys. Rev. B* **1976**, *13*, 1893–1902.
26. Chance, R. R.; Prock, A.; Silbey, R. Molecular Fluorescence and Energy Transfer Near Interfaces. *Adv. Chem. Phys.* **1978**, *37*, 1–65.
27. Henderson, B.; Hall, T. P. P. Some Studies of Cr^{3+} and Mn^{4+} Ions in Magnesium Oxide. *Proc. Phys. Soc.* **1967**, *90*, 511–518.
28. Altman, I. S.; Pikhisa, P. V.; Choi, M.; Song, H.-J.; Nasibulin, A. G.; Kauppinen, E. I. Zero-Phonon Lines in the Photoluminescence Spectra of MgO:Mn^{2+} Nanocrystals. *Phys. Rev. B* **2003**, *68*, 125324.
29. Altman, I. S.; Pikhisa, P. V.; Choi, M.; Jon, J. I.; Song, H.-J.; Agranovski, I. E.; Bostrom, T. E. Line Spectra from Doped Nano-Oxide: A Design for Nanooptics. *Appl. Phys. Lett.* **2003**, *83*, 3689–3691.

30. Iverson, M. V.; Silbey, W. A. Temperature Dependence of Ni^{2+} Luminescence in $KZnF_3$, MgF_2, and MgO. *J. Lumin.* **1979**, *20*, 311–324.
31. Schuller, J. A.; Karaveli, S.; Schiros, T.; He, K.; Yang, S.; Kymissis, I.; Shan, J.; Zia, R. Orientation of Luminescent Excitons in Layered Nanomaterials. *Nat. Nanotechnol.* **2013**, *8*, 271–276.
32. Zhu, W.; Wang, D.; Crozier, K. B. Direct Observation of Beamed Raman Scattering. *Nano Lett.* **2012**, *12*, 6235–6243.